Article

Self-Lubricating Effect of FeWO$_4$ Tribologically Synthesized from WC-(Fe-Mn-C) Composite during High-Speed Sliding against a HSS Disk

Nikolai Savchenko [ID], Irina Sevostyanova and Sergei Tarasov *[ID]

Institute of Strength Physics and Materials Science, 634055 Tomsk, Russia; savnick@ispms.ru (N.S.);
sevir@ispms.ru (I.S.)
* Correspondence: tsy@ispms.ru

Abstract: WC-(Fe-Mn-C) composites with γ-iron and $\gamma + \alpha'$ matrices were sintered and then tested at sliding speeds in the range 7–37 m/s. The coefficient of friction was exponentially reduced as a function of sliding speed reaching its minimum at 37 m/s. This behavior was provided by the mechanochemical formation of iron tungstate FeWO$_4$ on the worn surfaces of composite samples. The lubricating effect of iron tungstate did not, however, allow for a reduction in wear. The worn surface was represented by a 3–10 µm-thickness tribological layer composed of fine WC and iron particles cemented by FeWO$_4$. This layer provided the self-lubricating effect in high-speed (high-temperature) sliding because of its easy shear and quasi-viscous behavior. The underlying 25–65 µm of thickness layer was composed of only heat-affected WC and recrystallized iron grains.

Keywords: composite; lubrication; sliding; friction

1. Introduction

Reducing wear and friction under high-temperature sliding conditions, for example, inside internal combustion or jet engines, during the high-speed processing of metals, etc., requires the use of metal–ceramic composites that are resistant to high-temperature tribo-oxidizing [1–5]. However, tribo-oxidizing of the composite components can offer an adaptation mechanism that may provide a generation of oxidized mechanically mixed layers on the worn surfaces. These smooth tribological layers are capable of shielding the underlying material from fracture, deformation and adhesion wear. Sometimes, the generation of these mechanically mixed layers may mean enhancing the wear due to a sliding-assisted unfavorable phase or chemical transformations on the worn surfaces [1–5].

A positive approach in such a situation could be the adaptive, in situ generation of anti-friction oxide compounds on the worn surfaces in high-speed (high-temperature) sliding [1–5]. Retaining the composites' good tribological characteristics in a wide temperature range is an issue discussed in many papers devoted to high-temperature tribological applications [1–5]. Oxides possessing a low shear strength may be good candidates for the preparation of solid lubricants as components of anti-friction composites. These candidates may include, for example, tungsten trioxide WO$_3$ or oxygen-lean W$_n$O$_{3n-1}$ or W$_n$O$_{3n-2}$ Magneli phases [6]. Alternative materials may be double- and triple-mixed oxides formed on the worn surfaces during sliding, which are capable of friction reduction [7–12]. Many compounds are known at present, such as Cs$_2$WOS$_3$, Ag$_2$MoO$_4$, ZnMoO$_4$, etc., which can be used as high-temperature anti-friction components [7–12]. These or other compounds may form on the worn surfaces as films by means of tribo-oxidation from the components that were transferred or added to the sliding zone under specific speed and loading conditions, and then allow for a reduction in wear and friction.

The potential use of the Magneli phases or mixed oxides as anti-friction components in composites is a widely discussed issue. The first approach is to synthesize these phases

while sintering the composite, as reported in the example of $WO_{2.9}$ and $ZrO_2 + WO_{2.9}$ [6]. The second approach involves the in situ tribological synthesis of the self-lubrication compounds, such as, for example, in the case of the high-speed sliding WC/Hadfield steel composite against a HSS disk when smooth glassy films covered the worn surface and could reach a coefficient of friction (CoF) of as low as 0.07 due to the tribological in situ synthesis of anti-friction compound $FeWO_4$ [13,14].

WC-Fe composites possess good strength and wear resistance, as well as mechanical processability [13–18], and can be used as a base material for the preparation of hybrid composites whose initially metallic matrix is reinforced by ceramic compounds. Additional reinforcement of the metallic matrix can be achieved by the formation of extra phases. For example, alloying the steel with 4 and 20 wt. % Mn allowed $\gamma + \alpha'$ and pure γ matrices to be obtained, respectively [17]. Compared to the single γ-phase one, the heterophase $\gamma + \alpha'$ matrix allowed for improvements in a composite's compression strength and wear resistance due to the strain-induced $\gamma \rightarrow \alpha'$ transformation [17]. Under sliding conditions at 7–37 m/s, a mechanically mixed layer was generated on both composites, was composed of fine WC fragments, and oxidized binder and $FeWO_4$ mixed oxide, whose lubrication characteristics were not studied in detail [18]. Generally speaking, $FeWO_4$ should demonstrate lubrication properties as well as other tungstates, such as $ZnWO_4$ $CuWO_4$, etc. [7,8,11,12]. At the same time, with the exclusion of a few references [13,14,18–20], the literature search provided almost no results relating to the tribological performance of these compounds, although a lot of experiments were reported where both W and Fe were present in the rubbed materials.

This research is focused on studying the tribological behavior of WC-(Fe-Mn-C) composites with γ-iron (WC-Mn20) and $\gamma + \alpha'$ (WC-Mn4) matrices as future base for the preparation of metal–ceramic composites that can demonstrating the lubricating effect of $FeWO_4$ in high-speed (high-temperature) applications.

2. Materials and Methods

Metal matrix composites (MMC) WC-(Fe-Mn-C) were produced using melt infiltration of porous WC preforms in vacuum at T = 1350 °C, as described elsewhere [17]. The resulting MMCs were thus composed of 80 wt. % WC grains and 20 wt. % (Fe-Mn-C) matrix. The matrix was deliberately alloyed with Mn to obtain the resulting samples with Fe-Mn-C matrices that contained either 4 wt. % (WC-Mn4) or 20 wt. % of Mn (WC-Mn20).

The total amount of carbon in the matrix was about 0.8 wt. % for all samples. On infiltration, the samples were withdrawn from the vacuum furnace, heated to 1150 °C and then quenched in oil. The final sample dimensions were $5 \times 5 \times 7$ mm^3. Both MMCs shared the same microstructure type, with mean carbide grain size and interparticle space 2.7 ± 0.5 μm and 1.2 ± 0.2 μm, respectively (Figure 1a,c). The residual porosity was not higher 0.5%.

The XRD phase analysis showed the presence of HCP WC and FCC γ-iron in WC-Mn20, while, in WC-Mn4, the matrix additionally contained about $20 \pm 5\%$ of α'-martensite (Figure 1e).

Mechanical characteristics of the composites are given in Table 1. As follows from the Table 1, the compression strength and ductility of the WC-Mn4 composite were higher than those of WC-Mn20, which had higher microhardness.

Table 1. Mechanical characteristics of WC-(Fe-Mn-C) metal matrix composites.

Characteristics	WC-Mn4	WC-Mn20
Compression strength, MPa	4080 ± 50	3500 ± 50
Strain-to-fracture, %	7.8 ± 0.5	5.1 ± 0.5
Microhardness, MPa	7600 ± 200	$8200\pm$
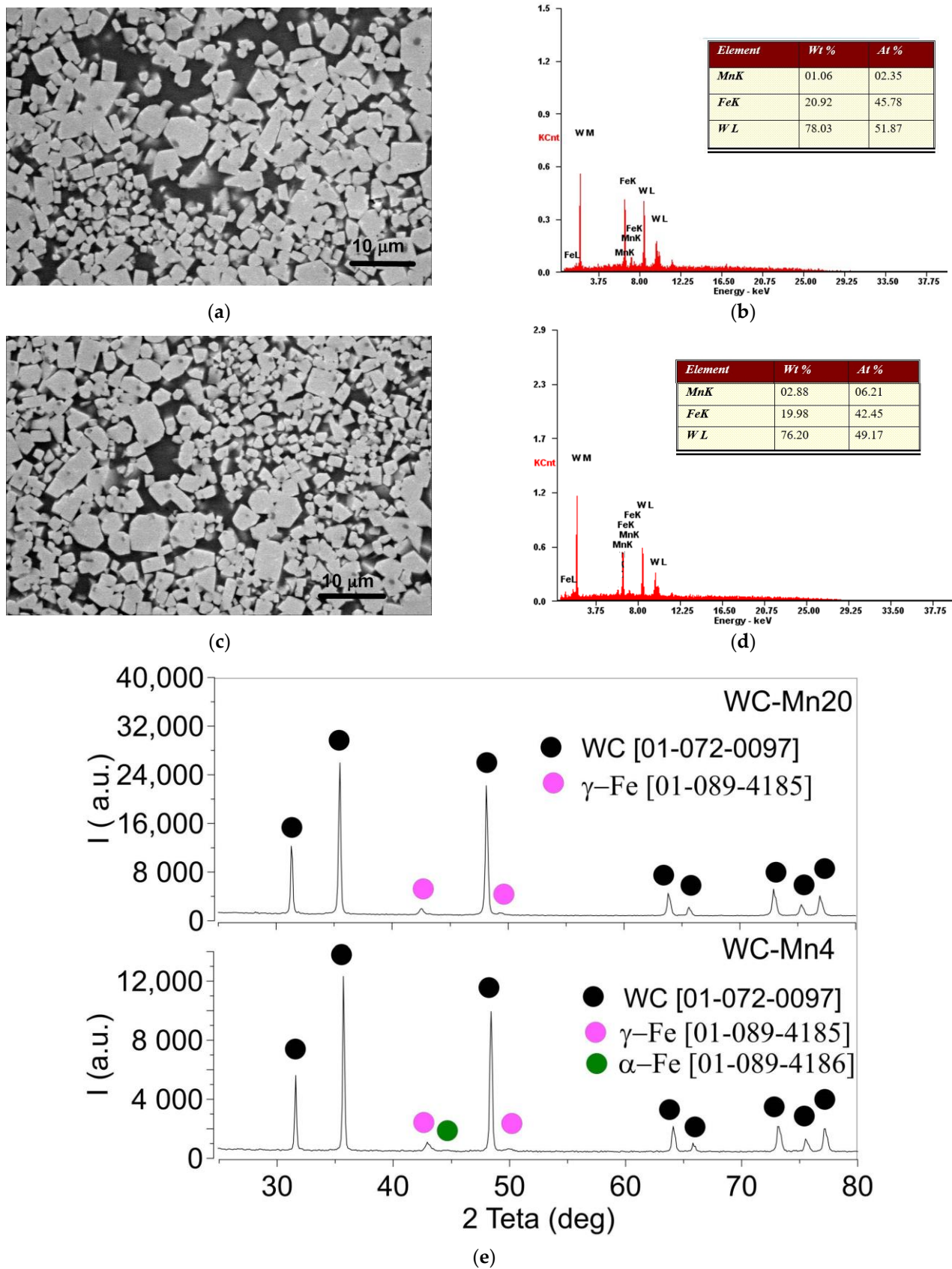
Figure 1. Microstructure (**a**,**c**), EDS spectra (**b**,**d**) and XRD patterns (**e**) of consolidated WC-Mn4 (**a**,**b**) and WC-Mn20 (**c**,**d**) composites.

Tribological pin-on-disk testing of the composites was carried out using a sliding test machine UMT-1 (Tochpribor, Ivanovo, Russia). A disk made of as-cast high-speed steel (HSS) 63–65 HRC steel disk was used as a counterbody. Microstructurally, the disk was composed of martensite with $M_{12}C$ carbides and small amount of the retained austenite. Chemical composition of the HSS M2 was as follows (wt. %): 15 V, 4.5 W, 3.6 Cr, 3.6 Mo, 1.8 Ni, 1.4 C, 1.0 Mn, Fe-balance). The disk track diameter was 240 mm. Tests were conducted at nominal contact pressure of 5 MPa (normal load 375 N divided by total three pins' contact area 75 mm² in the speed range of 7–37 m/s (7 m/s, 10 m/s, 20 m/s, 30 m/s, 37 m/s) at ambient conditions of approximately 25 °C and 40–50% relative humidity. Total three experiments (9 pins) each with wear path length 1000 m were conducted at each of the sliding speed values. Test duration diminished with the sliding speed growth so that, at 7, 10, 20, 30 and 37 m/s, test durations were 143 s, 100 s, 50 s, 33 s and 27 s, respectively.

Wear was evaluated by measuring the sample's height before and after the test and then calculating the wear rate as volume loss (mm³) divided by sliding path length (m)-mm³/m. Coefficient of friction (CoF) vs. time dependencies were obtained from experiments that demonstrated a steady sliding stage with moderate friction force oscillation amplitudes. These steady sliding portions of the curves were used to calculate the mean CoF values for each experiment.

Wear rate of the HSS disk was not evaluated but, given that the wear track length was about ~750 mm and tests' durations ranged from 143 s to 27 s depending on the sliding speed, we may see that the wear rate of the disk was negligible compared to that of a pin.

Flash temperatures on the worn surfaces were estimated using the well-known equation [21]:

$$\Delta T = \frac{\mu P V}{4J\left(K_{sample} + K_{disk}\right)\alpha} \tag{1}$$

where μ is the CoF, P and V are the normal load and sliding speed, respectively, K_{sample} and K_{disk} are thermal conductivities of the pin and disk, respectively. J is the Joule's constant (in this case, $J = 1$), and α is the contact radius of the real contact area to be determined from the following Equation (2):

$$\alpha = \left(\frac{P}{\pi H_{sample}}\right)^{1/2} \tag{2}$$

H_{sample} is the sample's hardness.

The results of this estimation are represented in Figure 2, together with the real temperatures of the sliding zone, as measured using a pyrometer. Really high flash temperatures occur on the real contact spots, and then the heat is dissipated to the bulk of the sample, somewhat increasing its average temperature. The latter can be measured using the pyrometer.

Both worn surfaces and wear debris were examined using a SEM instrument Philips SEM-515 attached with an EDS analyzer EDAX ECON IV (Koninklijke Philips Electronics N.V., Amsterdam, The Netherlands). XRD was carried out using X-ray diffractometer DRON-7 (Burevestnik, Saint-Petersburg, Russia), Cu-Kα obtained at 40 kV and 22 mA with a scan range of 15–102° with (2θ) step size of 0.05° and counting time of 10 s. XRD peak. Identification of the XRD reflections was performed using Crystal Impact's software "Match!" (version 3.9, Crystal Impact, Bonn, Germany).
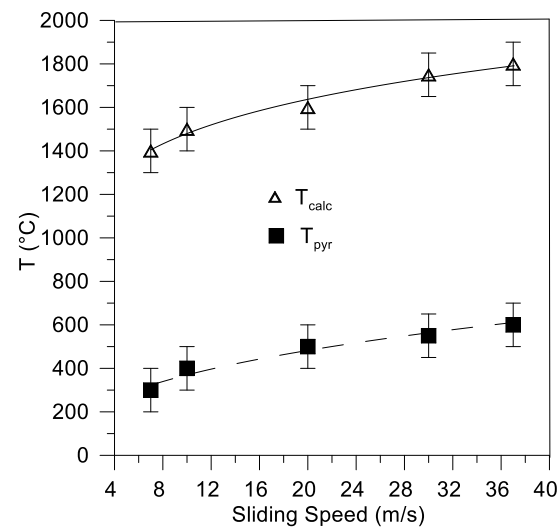
Figure 2. Temperatures of sliding zone according to pyrometer, as calculated from Equations (1) and (2).

3. Results

3.1. Wear and Friction Characteristics

There was not much difference between the WC-Mn4 and WC-Mn20 in terms of wear rate vs. sliding speed dependencies when tested in the sliding speed range from 7 to 10 m/s. The wear was characterized by mild intensity until the sliding speed of 20 m/s was reached, at which point wear rate started increasing sharply. WC-Mn20 demonstrated its wear rate to be almost three times higher than that of the WC-Mn4 (Figure 3a).
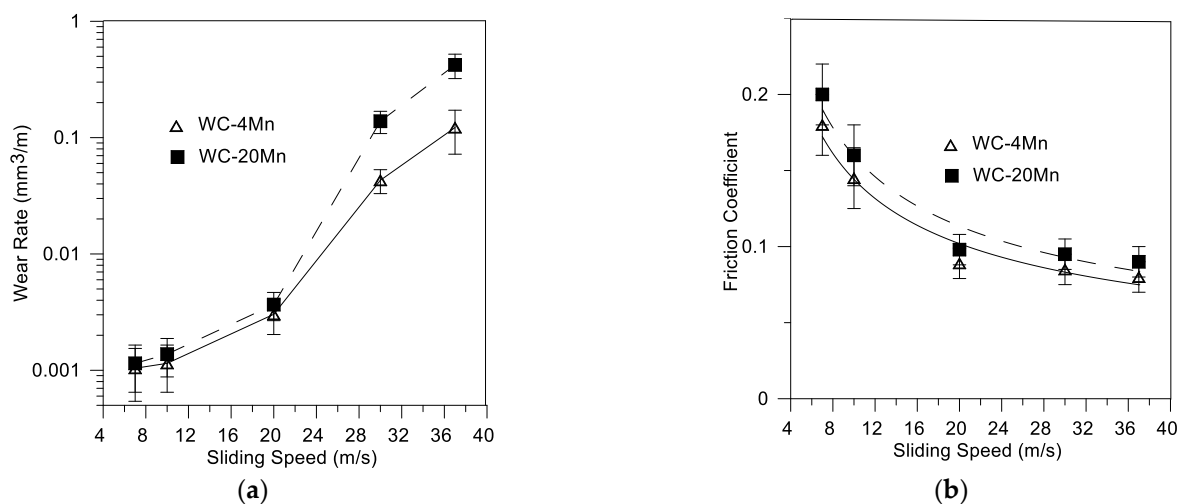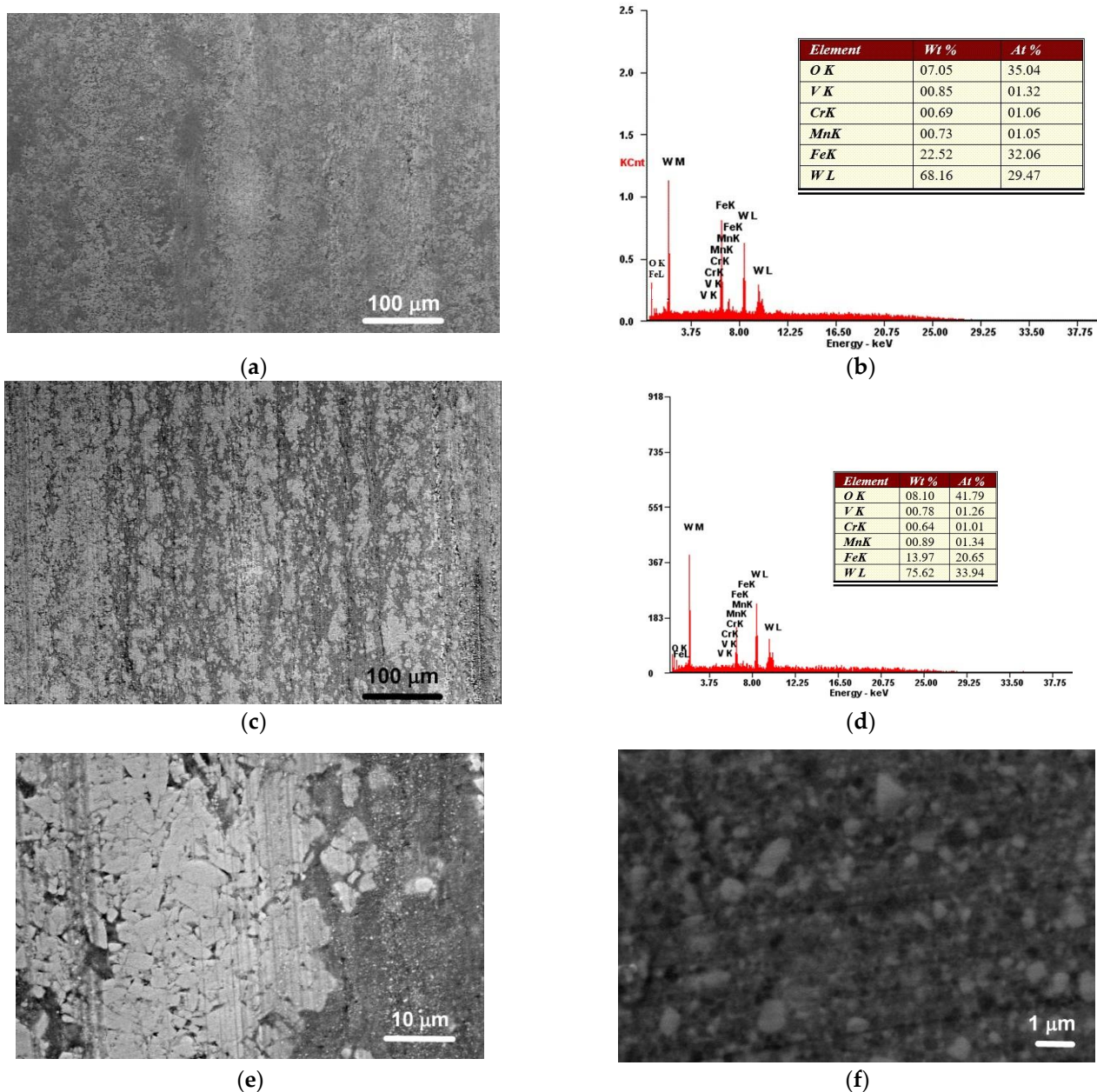

Figure 3. Wear rate (**a**) and coefficient of friction (**b**) dependencies of WC-Mn4 and WC-Mn20 on the sliding speed.

Both composites demonstrated that their CoF values reduced with the increasing sliding speed (Figure 3b). WC-Mn4 demonstrated a lower CoF than that of WC-Mn20 for all sliding speeds. Both composites demonstrated a rather steady sliding stage with moderate friction force oscillation amplitudes.

3.2. Worn Surface Analysis

Worn surfaces of both composites are characterized by the presence of bright and grey SEM SE areas, elongated with respect to the sliding direction (Figures 4a,c and 5a). Bright contrast areas were identified as WC grains and fragments, which were agglomerated and

compacted in the course of sliding against the steel disk (Figure 4e). The grey ones appear to be oxidized transfer layer areas (TLA), which incorporate small WC fragments and lie on the base composite structures (Figure 4f).

Element	Wt %	At %
O K	07.05	35.04
V K	00.85	01.32
CrK	00.69	01.06
MnK	00.73	01.05
FeK	22.52	32.06
W L	68.16	29.47

(a)   (b)

Element	Wt %	At %
O K	08.10	41.79
V K	00.78	01.26
CrK	00.64	01.01
MnK	00.89	01.34
FeK	13.97	20.65
W L	75.62	33.94

(c)   (d)

(e)   (f)

Figure 4. Typical worn surfaces of WC-(Fe-Mn-C) composites observed after sliding at 37 m/s: WC-Mn4 (**a**,**e**,**f**) and WC-Mn20 (**c**). Compacted carbide areas (**e**) and TLA areas (**f**). EDS spectra of worn surface WC-Mn4 (**b**) and WC-Mn20 (**d**).
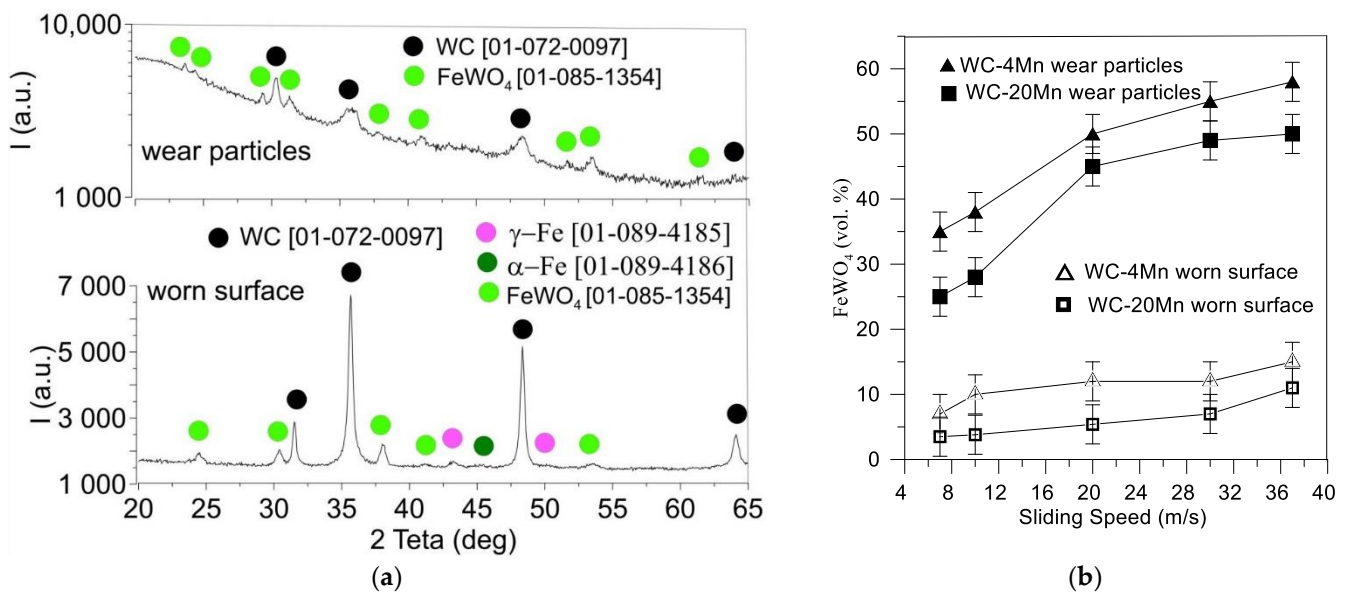
EDS spectra were obtained from the worn surfaces of WC-Mn4 and WC-Mn20 (Figure 4b,d) composites, which allowed for the presence of oxygen, vanadium and chromium to be observed, i.e., elements that did not belong to the as-sintered composites (Figure 1b,d) but could be oxidized and transferred from the counterbody disk. The worn surface of the WC-Mn20 composite can be characterized by its lower amount of iron as compared to that of the WC-Mn4 (Figure 4b,d). Furthermore, the worn surfaces of both WC-Mn4 and WC-Mn20 composites were depleted by Mn as compared to those of as-sintered samples (Figure 1b,d).
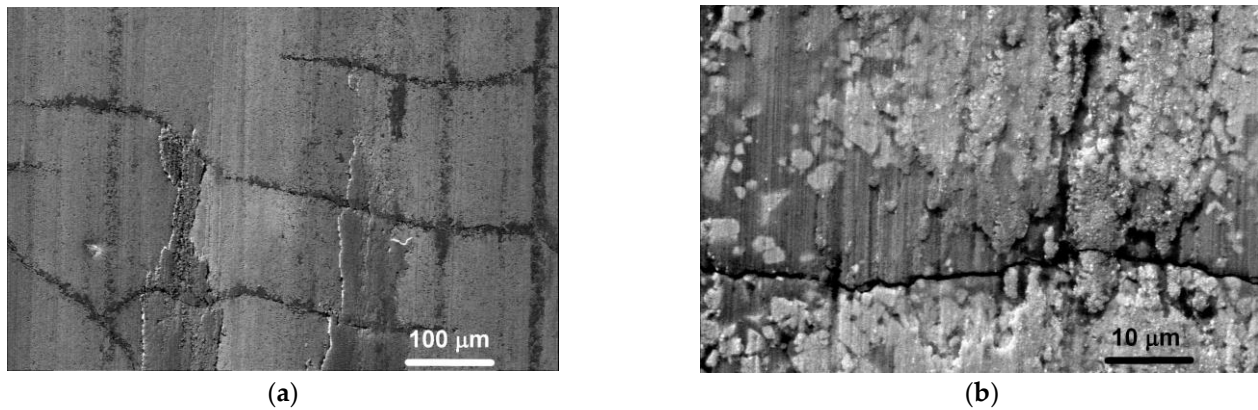
Figure 5. Typical Cracks (**a**) and carbide fragments (**b**) on the worn surface of WC-(Fe-Mn-C) composites formed after sliding at 7–20 m/s presented by the example of WC-Mn20 tested at 20 m/s.

Sliding at speeds in the 7–20 m/s range resulted in the generation of a system of transversal cracks (Figure 5), while no cracks were noticed on the worn surfaces of samples tested at 30 m/s and 37 m/s (Figure 4a,c).

XRD patterns were obtained from the worn surfaces of all samples that allowed for the identification of phases such as WC, $FeWO_4$, γ-iron and α-iron in WC-Mn4, and only γ-iron in WC-Mn20 (Figure 6a). The XRD patterns were also obtained from collected and compacted wear debris to demonstrate the presence of only two phases, such as WC and $FeWO_4$ (Figure 6a). The iron tungstate $FeWO_4$ can be the result of the in situ tribooxidation of WC in the presence of steel transferred from the disk during sliding.


Figure 6. XRD patterns of wear debris and worn surfaces of WC-Mn4 tested at 20 m/s (**a**) and $FeWO_4$ content vs. sliding speed dependencies obtained from a semi-quantitative analysis of corresponding XRD peaks from the worn surfaces and wear debris (**b**).

In this connection, all the XRD patterns were analyzed for $FeWO_4$ peak intensities obtained on both composites and different sliding speeds (Figure 6a). The results of this analysis are presented in Figure 6b, where dependencies characterize the amounts of the $FeWO_4$ that were detected on the worn surfaces and in corresponding wear debris. Let us assume that these dependencies characterize the amount of the tungstate produced during the tribooxidation of samples. If so, then the amounts of $FeWO_4$ grow, as expected, with the sliding speed (temperature) and provide a friction reduction effect, as shown in Figure 3b.

The maximum $FeWO_4$ concentrations were detected in wear debris collected from both samples. Lower $FeWO_4$ concentrations are present on the worn surfaces. In addition, it seems that higher amounts of $FeWO_4$ were produced by the tribo-oxidation of WC-Mn4 than WC-Mn20 at all sliding speeds.

A layer-by layer XRD with the successive removal of 10–20 μm layers by grinding was carried out to study the structural changes that occurred below the worn surfaces. Plastic strain penetration was evaluated by reconstructing the dependencies of sizes of coherent scattering area sizes (CAS) and micro-distortions of the WC grains on the distance below the worn surface (Figure 7a,b). It can be seen that both these microstructural parameters demonstrate changes up to a plateau, starting ~60 μm below the worn surface. This finding allows for the suggestion that all sliding-induced structural changes are limited inside the ~60 μm subsurface layer, i.e., plastic deformation penetration was not deeper ~60 μm below the worn surface (Figure 7a–c). It can be observed from Figure 7c that plastic deformation penetration reached its maximum at 20 m/s for both types of composites, at which point their wear rate vs. sliding speed dependencies started to fall apart (Figure 3a). However, in the range 20–37 m/s, the WC-Mn20 composite shows a deeper strain penetration and higher wear rate than that of WC-Mn4. This finding can be related to the different phase compositions and the strengths of their matrices.

(a)

(b)

(c)
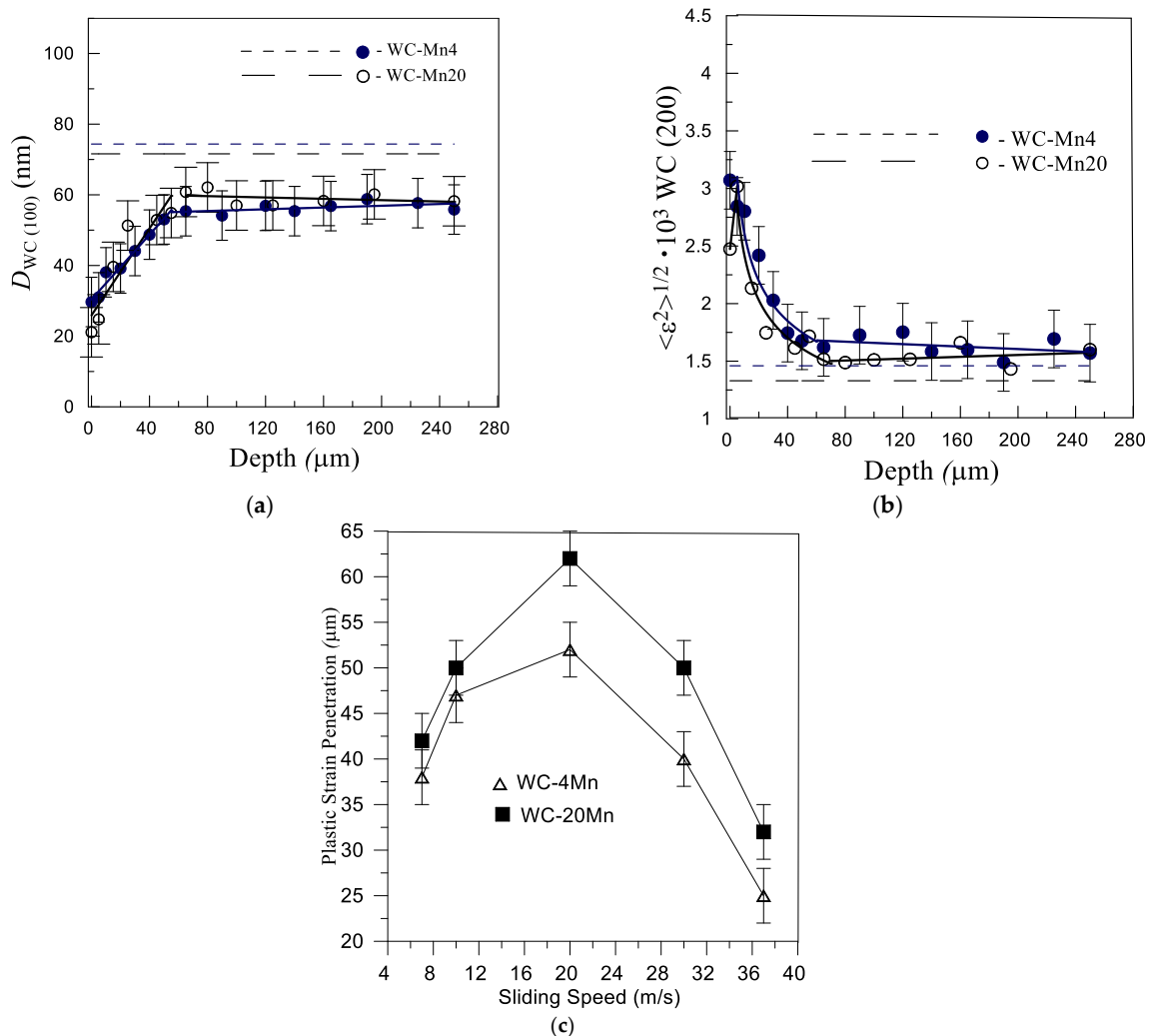
Figure 7. The WC grain parameters such as CSA size (**a**) and micro-distortions (**b**) vs. distance below the worn surface after sliding at 20 m/s. Evolution of the plastic strain penetration with sliding speed on WC-Mn4 and WC-Mn20 (**c**). Dotted lines in Figure 7a,b identify levels of CSA size and micro-distortions inherent in the as-sintered composites.

Subsurface changes in WC grains can be seen in Figure 8a,b as partly oxidized dark portions of the grains with patches of mechanically mixed layers in the top parts. Increasing the sliding speed from 7 to 37 m/s resulted in the generation of a 3–10-μm thickness tribological layer on the worn surfaces of both WC-Mn4 and WC-Mn20 composites. This layer was composed of fine WC and iron particles cemented by $FeWO_4$.
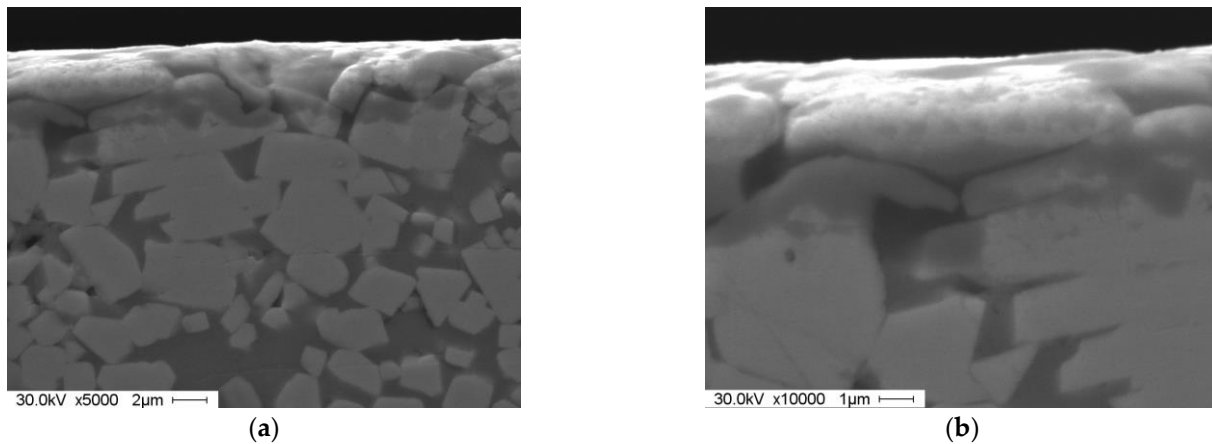
Figure 8. Subsurface oxidation of WC grains (**a**) and mechanically mixed layer (**b**) on the worn surface of WC-Mn4 composite tested at 20 m/s.

3.3. Wear Particles

A metallographic examination of wear debris showed at least two morphological types, such as platy fragments (Figure 9a) and irregularly shaped clinker-type (bubbles) debris (Figure 9b). The latter looked as if it was composed of 0.1–10-μm-sized semispherical asperities. As the fragments of the worn surface layer, the platy particles clearly showed their top and bottom surfaces to be flat and irregularly shaped, respectively.
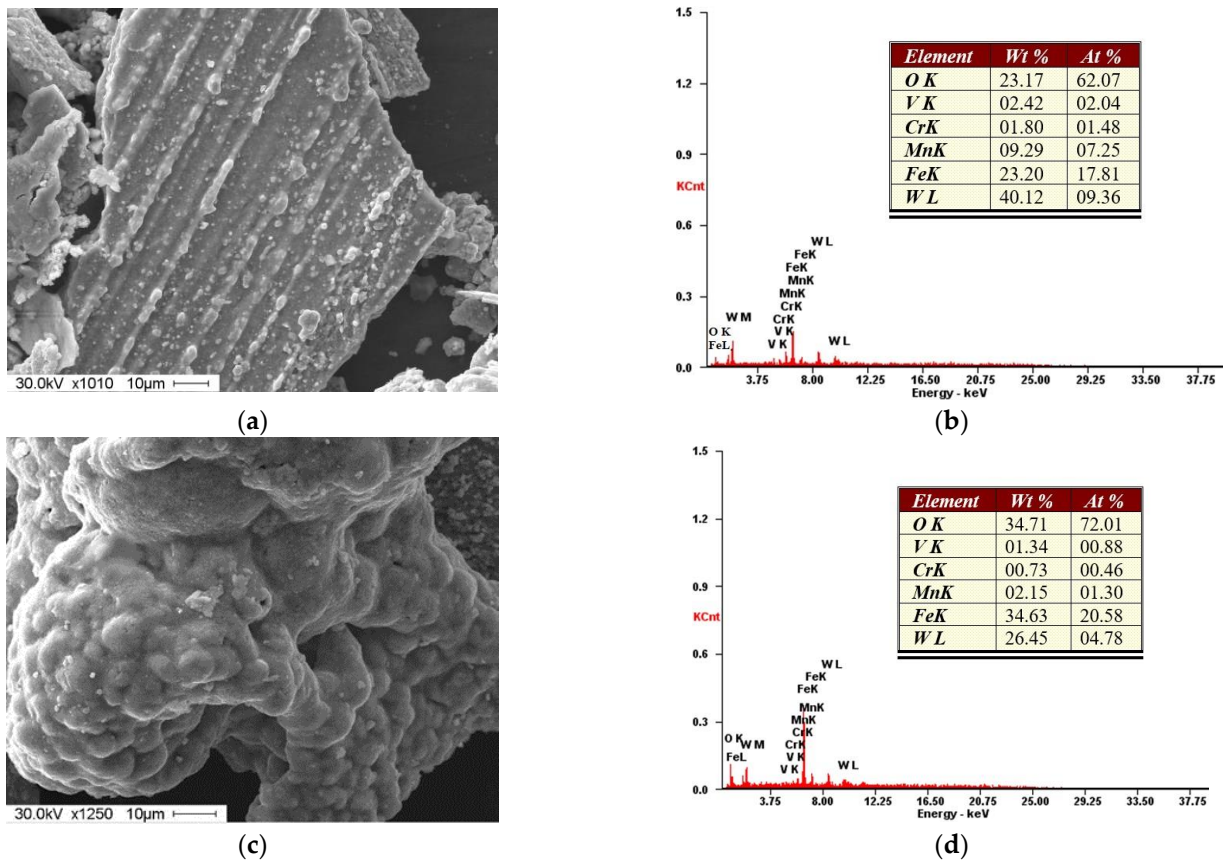
The EDS spectra obtained from wear debris collected from the worn surfaces of both WC-Mn4 and WC-Mn20 composites (Figure 9b,d) showed the presence of elements such as O, V, and Cr, i.e., the oxidized elements comprising the counter-body steel. When comparing the EDS spectra of these wear debris with those obtained from the corresponding worn surfaces (Figure 4b,d), one can conclude that the wear debris contain more oxygen and less tungsten with a relatively high iron content. The worn surface of the WC-Mn20 composite can be characterized by a lower amount of iron as compared to that of WC-Mn4 (Figure 4b,d).

The clinker-type wear debris contained less W as compared to that of platy particles (Figure 9b,d). The platy fragments of WC-Mn20 are characterized by a Fe higher content compared to that of WC-Mn4.

The percentages of platy fragments and clinker particles depend on the sliding speed, as shown in Figure 10. More clinker-type particles are formed when increasing the sliding speed and, consequently, the sliding zone temperature. In fact, the platy fragments can also bear $FeWO_4$ asperities or even ridges on their worn surfaces (Figure 9a).

Cross-section SEM BSE image of a clinker-type particle allows for the observation of inner voids, as well as a different contrast between its core structures and shell (Figure 11a). The framework's solid structures are composed of fine 0.1–0.3 μm particles (Figure 11b).
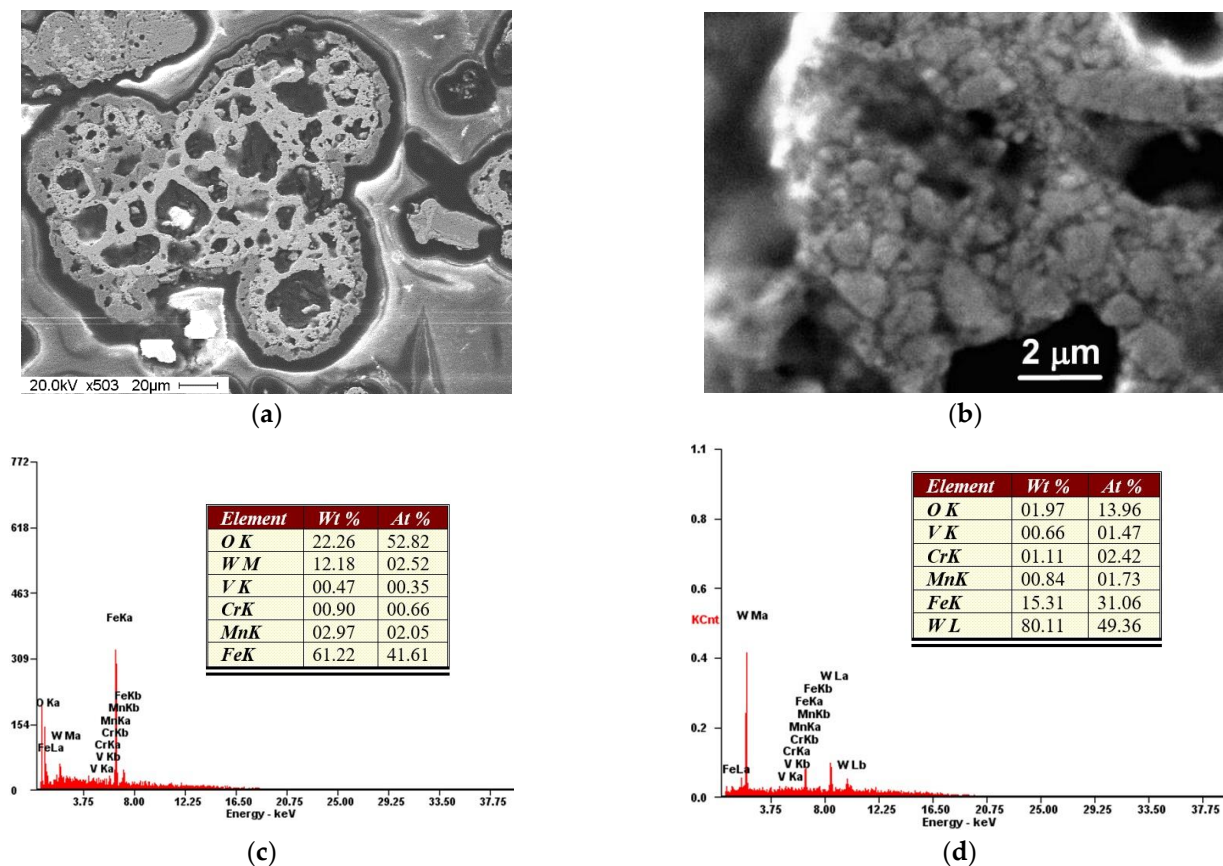
Considering the EDS spectra (Figure 11c,d), it was suggested that the clinker-type particles can be formed by intermixing $FeWO_4$ with fine carbide wear debris.

Element	Wt %	At %
O K	23.17	62.07
V K	02.42	02.04
CrK	01.80	01.48
MnK	09.29	07.25
FeK	23.20	17.81
W L	40.12	09.36

Element	Wt %	At %
O K	34.71	72.01
V K	01.34	00.88
CrK	00.73	00.46
MnK	02.15	01.30
FeK	34.63	20.58
W L	26.45	04.78

Figure 9. Morphological types and EDS spectra of wear particles as platy fragments (**a**,**b**) and clinker-type (bubbles) particles (**c**,**d**). Wear particles were obtained by collecting them after sliding WC-Mn20 composites at 20 m/s.
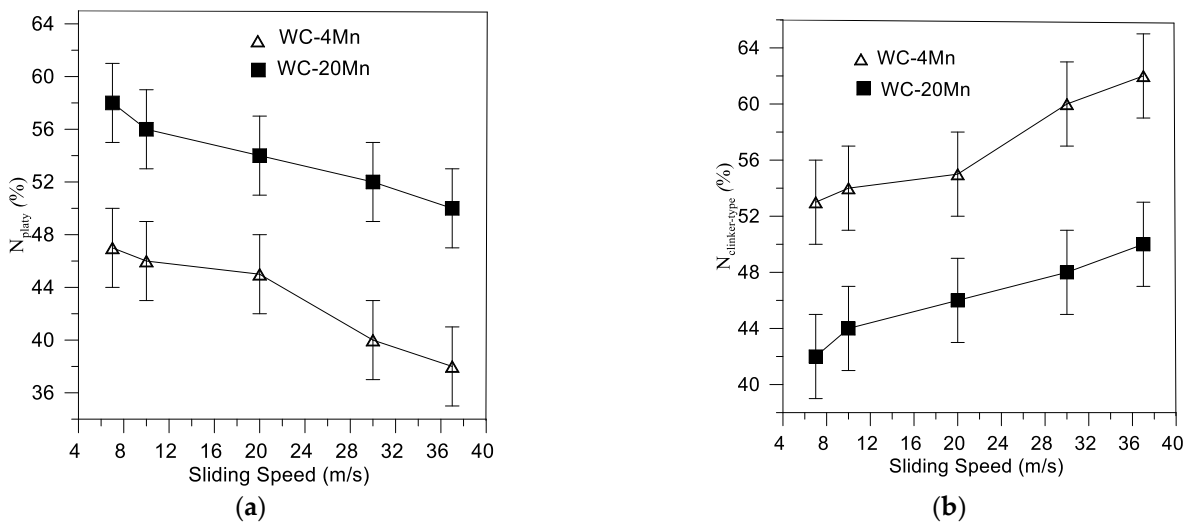
Figure 10. Percentages of platy (**a**) and clinker-type (**b**) wear particles vs. sliding speed.

(a)

(b)

Element	Wt %	At %
O K	22.26	52.82
W M	12.18	02.52
V K	00.47	00.35
Cr K	00.90	00.66
Mn K	02.97	02.05
Fe K	61.22	41.61

(c)

Element	Wt %	At %
O K	01.97	13.96
V K	00.66	01.47
Cr K	01.11	02.42
Mn K	00.84	01.73
Fe K	15.31	31.06
W L	80.11	49.36

(d)

Figure 11. Cross-section view of the clinker-type particle (**a**) and microstructure of the inner framework (**b**). (**c**) EDS spectrum of dark shell, (**d**) EDS spectrum of bright core. Clinker-type particles were obtained after sliding WC-Mn20 composites at 20 m/s.

4. Discussion

The results of this work clearly show that the coefficient of friction is reduced with increasing sliding speed and, correspondingly, the sliding zone temperatures. On the other side, the WC-(Fe-Mn-C) composites produce iron tungstate over the course of high-speed sliding against a HSS disk. The tungstate can serve as a high-temperature lubricant and, therefore, reduce friction between the pin and disk. When sliding the WC-(Fe-Mn-C) composites at 30 and 37 m/s with a contact pressure of 5 MPa against the steel counter-body, it was possible to generate a tribological transfer layer composed of fine WC fragments and iron-rich particles, cemented by mechanochemically formed $FeWO_4$. Such a composite layer can absorb dynamic loads, reducing friction (Figure 3b) and forming a smooth protection for the underlying composite grains against deformation and fracture (Figure 4a,c,e,f). Such an effective protection layer could not appear in sliding at lower speeds (lower temperatures); therefore, the worn surfaces of both composites experienced subsurface fractures (Figure 5) and deformation (Figure 7).

Let us consider the mechanochemical aspects and conditions that could facilitate the iron tungstate synthesis during the high-speed sliding of WC-(Fe-Mn-C) composites. Tungsten carbide becomes prone to intense oxidizing at temperatures above 800 °C [22]. This oxidizing can occur according to the reactions, as follows:

$$WC + 2O_2 \rightarrow WO_3 + CO \tag{3}$$

The presence of Fe-Mn-C matrix and the transferred HSS components may also oxidize their main component, iron, according to the following reaction:

$$2Fe + O_2 \rightarrow 2FeO \tag{4}$$

The occurrence of this reaction can be facilitated by accumulating structural defects and plastic strain in the subsurface of the composite matrix. The higher the plastic deformation penetration into the sample, the more intense the tribooxidation. The preferable reaction to produce iron tungstate over the course of high-speed sliding could be as follows [20]:

$$FeO + WO_3 \rightarrow FeWO_4 \tag{5}$$

The amount of iron tungstate depends on the sliding speed and type of WC-(Fe-Mn-C) composite. According to the results obtained from semi-quantitative XRD, the amount of iron tungstate on the worn surface is lower than that detected in wear debris (Figure 6b). This finding can be explained by the fact that the tungstate produced by tribo-oxidation is increased with the sliding speed and temperature, along with the intensification of wear, so that more tungstate is carried away with the debris and solidify there as porous particulates. Simultaneously, effective friction reduction occurs with increases in the sliding speed (Figure 3b).

The cross-section views of the clinker-type particles with their thin inner walls (Figure 11a,b) suggest that these particles could not originate directly from mechanical wear as wear debris. They are instead the product of tribo-chemical reactions when hot crushed WC fragments react with oxygen and oxidized iron, according to reactions (3), (4), and (5). The gaseous reaction product CO may form bubbles with the $FeWO_4$, intermixed with the WC fragments and transferred iron oxide particles.

A corresponding tribology literature search was carried out to look for similar types of hollow particles; however, no relevant references were found. However, numerous papers are devoted to studying tribo-chemical alloying or even the synthesis of compounds in attritors [23]. It is not inconceivable that this type of particle can be formed by tribo-chemical synthesis, but the interests of researchers specializing in this field lie more with studying the phases and compositions of the compounds, rather than their particle structure and morphology. Therefore, to the best of our knowledge, we could not find any descriptions of these specific particulates in the literature.

A higher amount of Mn was detected in wear debris (Figures 9b,d and 11c) than in the steel counter-body. This finding suggests that a steel matrix of the WC-(Fe-Mn-C) plays the main role in the tribooxidation and generation of $FeWO_4$.

There were no qualitative differences between the worn surfaces on WC-Mn4 and WCMn20 composites obtained at the same sliding speed (Figure 4a,c) despite the difference in wear rate, which, in fact, increased with the sliding speed (Figure 3a). The worn surface cracking was less or not noticeable on samples tested at higher speeds, irrespective of the composite matrix (Figures 4c and 5a), i.e., sliding speed was the main factor defining the worn surface morphology.

It was shown earlier [17] that the WC-Mn4 composite had a lower wear rate when sliding at the 1–4 m/s speed range as compared to that of WC-Mn20, and this difference was related to the fact that the WC-Mn4 had a meta-stable double phase ($\gamma + \alpha'$) matrix that experienced strain-induced $\gamma \rightarrow \alpha'$ transformation and hardening during sliding. Such a suggestion can be true only in the case of low frictional heating, while high-speed sliding generates much more heat, so the $\alpha' \rightarrow \gamma$ transformation becomes more real. Under these conditions, the double-phase WC-Mn4 matrix would demonstrate a higher resistance to plastic deformation, and thus more effectively retain the carbide grains until the moment of complete $\alpha' \rightarrow \gamma$ transformation. By this time, however, the γ-phase matrix of the WC-Mn20 composite would be thermally softened and not capable of retaining the WC grains in place.

The EDS data obtained from the worn surfaces (Figure 4d) and wear debris (Figure 9b,d) of the WC-Mn20 composite demonstrate that the worn surfaces are enriched with WC as compared to the base metal (Figure 1d), while wear debris contain more metallic components.

As follows from Figure 10b, the clinker/platy particle ratio grows with the sliding speed. Additionally, the number of clinker-type particles is higher for the WC-Mn4. Considering the dependence of $FeWO_4$ on sliding speed (Figure 6b), one may suggest that

the clinker-type particles are mainly formed of $FeWO_4$. It seems that the worn surface of WC-Mn4 is more successful in synthesizing and retaining the iron tungstate film at high sliding speeds.

It was mentioned above that both WC-Mn4 and WC-Mn20 composites are intended for the preparation of hybrid ceramic–metal matrix composites and, therefore, their wear resistance should be considered and compared with those of other candidates, such as WC-30 wt. % Hadfield steel [14], Y-TZP [24], Y-TZP + 20 wt. % Al_2O_3, and ZrB_2 + 20 vol.% SiC [4].

For that purpose, the wear rate and CoF values of all these composites were obtained in sliding at 37 m/s and contact pressure 5 MPa against the HSS disk, with other tribological experiment conditions kept identical to those used in the present work [4,14,24].

A reduction in friction was achieved for ZrB_2 + 20 vol.% SiC due to the formation of a liquid phase that served as a liquid lubricant at high temperatures [4,5]. The Y-TZP-base ceramics such as Y-TZP and Y-TZP 20 wt. % Al_2O_3 demonstrated a relatively high wear resistance due to subsurface deformation by means of ferroelasticity mechanism, accompanied by the subsurface layer deformation texturing and generation of a protection transfer layer [24,25].

The CoF values for both WC-Mn4 and WC-Mn20 at 30 m/s and 37 m/s were at the level of ~0.08 i.e., almost twice as low as ~0.2 inherent with Y-TZP, Y-TZP + 20 wt. % Al_2O_3 and ZrB_2 + 20 vol.% SiC ceramics but comparable to the CoF value demonstrated by WC-30 wt. % Hadfield steel metal ceramic composites discussed above (Figure 12a) [4,14,25].
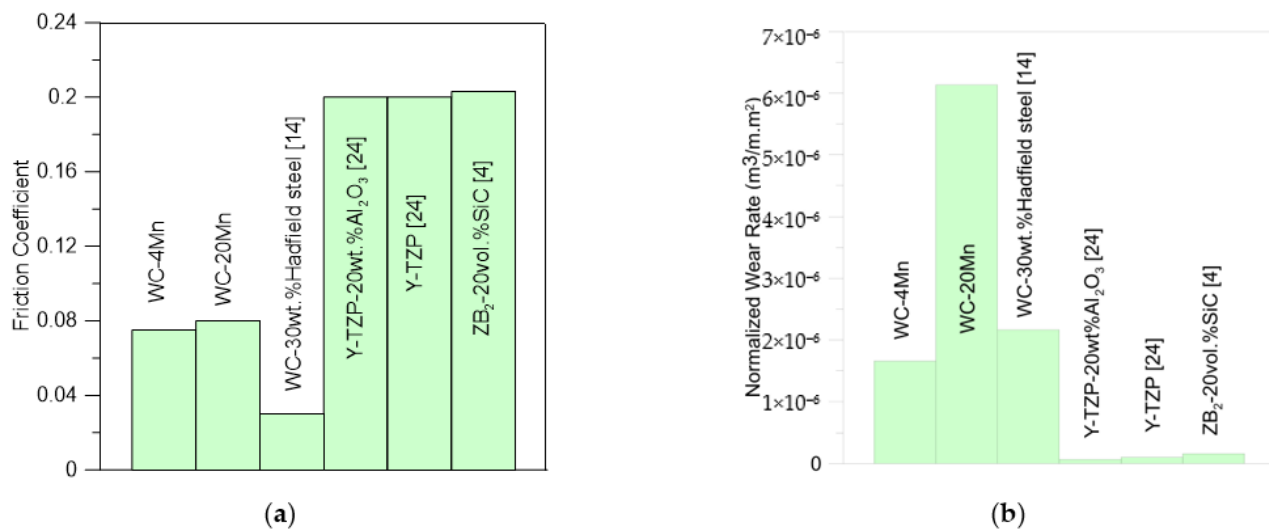
Figure 12. Friction coefficient (**a**) and normalized wear rate (**b**) for different composites tested at sliding speed 37 m/s and contact pressure 5 MPa.

A series of works were published regarding the sliding of the MAX-phase composites over steel counter-bodies when CoF values were obtained under the following conditions: f~0.15 at 30 m/s and 30 N [26]; f~0.22 at 30 m/s and 20 N [27]; f~0.13 at 30 m/s and 80 N [28]; f~0.25 at 30 m/s and 60 N [29]. A comparison between the above data and CoF values obtained in the present study, namely, ~0.08, shows that both WC-Mn4 and WC-Mn20 are good candidates for the hybrid composites.

To provide a correct comparison between the wear rate values obtained on WC-Mn4 and WC-Mn20 and those obtained on the above-mentioned materials (Figure 12b), the normalized wear rate values were calculated as wear rate divided by the apparent contact area [30]. It was also impossible to overlook the high wear rate of the metal ceramic composites such as WC-30 wt. %Hadfield steel, WC-Mn4 and WC-Mn20 during sliding at high speeds (Figure 12b). A relatively high content of metal matrix in the composite may result in the selective wear of the thermally softened and even partly melted matrix.

It could be suggested that $FeWO_4$ is effective for high-speed (temperature) lubrication in sliding against steel. This result may be used for to develop self-lubricating composites by replacing part of the metal matrix with ceramics in an attempt to reduce wear in the base ductile WC-reinforced ferrous matrix composites. Y-TZP)/alumina-reinforced ceramic matrix could be a good candidate, since all the components, such as WC, ZrO_2, Al_2O_3 and steel, can be consolidated into a bulk composite [31]. The Y-TZP-Al_2O_3 can also be additionally reinforced by adding WC cemented by high-manganese steel. These approaches would allow for the use of both mechanical reinforcement and tribological adaptation by the in situ synthesis of $FeWO_4$ of the bulk composites for high-temperature tribological applications.

5. Conclusions

WC-(Fe-Mn-C) composites with γ-iron (WC-Mn20) and $\gamma + \alpha'$ (WC-Mn4) matrices were sintered as base materials for the future fabrication of a hybrid ceramic–matrix composite with dispersed steel particles for tribological applications. The tribological behavior of the WC-(Fe-Mn-C) was studied in sliding against a HSS disk. The effect of tribological adaptation provided by the tribological generation of a tribological composite protection self-restored layer composed of fine WC fragments and iron-rich wear debris cemented by an in situ, high-speed sliding synthesized $FeWO_4$ compound has been discovered. Both composites demonstrated that their CoF values reduce with increasing sliding speed due to the anti-friction behavior of the tribological layer in situ, formed of wear debris and $FeWO_4$. WC-Mn4 demonstrated a lower CoF than that of WC-Mn20 for all sliding speeds. The amount of $FeWO_4$ grow with the sliding speed (temperature), as expected, and provided a reduction in friction. The maximum $FeWO_4$ concentrations were detected in the wear debris of both samples. Fewer values were determined for the worn surfaces. It also seems that higher amounts of $FeWO_4$ were produced by the tribooxidation of WC-Mn4 than WC-Mn20 at all sliding speeds.

Institutional Review Board Statement: Not applicable.

Informed Consent Statement: Not applicable.

Data Availability Statement: Data sharing is not applicable to this article.

Conflicts of Interest: The authors declare no conflict of interest.

References

1. Kumar, R.; Antonov, M. Self-lubricating materials for extreme temperature tribo-applications. *Mater. Today Proc.* **2020**, *44*, 4583–4589. [CrossRef]
2. Zhai, W.; Bai, L.; Zhou, R.; Fan, X.; Kang, G.; Liu, Y.; Zhou, K. Recent Progress on Wear-Resistant Materials: Designs, Properties, and Applications. *Adv. Sci.* **2021**, *8*, 2003739. [CrossRef]
3. Torres, H.; Ripoll, M.R.; Prakash, B. Tribological behaviour of self-lubricating materials at high temperatures. *Int. Mater. Rev.* **2017**, *63*, 309–340. [CrossRef]
4. Savchenko, N.L.; Mirovoy, Y.A.; Buyakov, A.S.; Burlachenko, A.G.; Rudmin, M.A.; Sevostyanova, I.N.; Buyakova, S.P.; Tarasov, S.Y. Adaptation and self-healing effect of tribo-oxidizing in high-speed sliding friction on ZrB_2-SiC ceramic composite. *Wear* **2020**, *446–447*, 203204. [CrossRef]
5. Savchenko, N.L.; Mirovoy, Y.A.; Burlachenko, A.G.; Sevostyanova, I.N.; Buyakov, A.S.; Rudmin, M.A.; Vorontsov, A.V.; Buyakova, S.P.; Tarasov, S.Y. Subsurface multilayer evolution of ZrB_2-SiC ceramics in high-speed sliding and adhesion transfer conditions. *Wear* **2021**, *482–483*, 203956. [CrossRef]

6. Cura, M.E.; Trebala, M.; Ge, Y.; Klimczyk, P.; Hannula, S.-P. Mechanical and tribological properties of $WO_{2.9}$ and $ZrO_2 + WO_{2.9}$ composites studied by nanoindentation and reciprocating wear tests. *Wear* **2021**, *478–479*, 203920. [CrossRef]

7. Zhu, S.; Cheng, J.; Qiao, Z.; Yang, J. High temperature solid-lubricating materials: A review. *Tribol. Int.* **2019**, *133*, 206–223. [CrossRef]

8. Kumar, R.; Hussainova, I.; Rahmani, R.; Antonov, M. Solid Lubrication at High-Temperatures—A Review. *Materials* **2022**, *15*, 1695. [CrossRef]

9. Kharanzhevskiya, E.V.; Ipatov, A.G.; Krivilyov, M.D.; Makarov, A.V.; Gil'mutdinov, F.Z.; Volkova, E.G. Ultralow friction behaviour of B_4C-BN-MeO composite ceramic coatings deposited on steel. *Surf. Coat. Technol.* **2020**, *390*, 125664. [CrossRef]

10. Kharanzhevskiy, E.V.; Ipatov, A.G.; Makarov, A.V.; Gil'mutdinov, F.Z.; Soboleva, N.N.; Krivilyov, M.D. Tribological performance of boron-based superhard coatings sliding against different materials. *Wear* **2021**, *477*, 203835. [CrossRef]

11. Voevodin, A.A.; Muratore, C.; Aouadi, S.M. Hard coatings with high temperature adaptive lubrication and contact thermal management: Review. *Surf. Coat. Technol.* **2014**, *257*, 247–265. [CrossRef]

12. Pervikov, A.; Filippov, A.; Mironov, Y.; Kalashnikov, M.; Krinitcyn, M.; Eskin, D.; Lerner, M.; Tarasov, S. Microstructure and properties of a nanostructured W-31 wt % Cu composite produced by magnetic pulse compaction of bimetallic nanoparticles. *Int. J. Refract. Met. Hard Mater.* **2022**, *103*, 105735. [CrossRef]

13. Savchenko, N.L.; Sevostyanova, I.N.; Utyaganova, V.R.; Gnyusov, S.F. High speed sliding of a WC/Hadfield steel composite against steel. *AIP Conf. Proc.* **2018**, *2053*, 040085. [CrossRef]

14. Savchenko, N.L.; Gnyusov, S.F.; Kul'kov, S.N. Structures formed during the friction of a metal-ceramic composite on steel under high-velocity sliding conditions. *Tech. Phys. Lett.* **2009**, *35*, 107–110. [CrossRef]

15. Gee, M.G.; Grant, A.; Roebuck, B. Wear mechanisms in abrasion and erosion of WC/Co and related hardmetals. *Wear* **2007**, *263*, 137–148. [CrossRef]

16. Humphry-Baker, S.A.; Vandeperre, L.J.M. Creep deformation of WC hardmetals with Fe-based binders. *Int. J. Refract. Met. Hard Mater.* **2021**, *95*, 105462. [CrossRef]

17. Sevostyanova, I.N.; Savchenko, N.L.; Kul'kov, S.N. Structural and Phase Binder State and Behavior during Friction of WC–(Fe–Mn–C) Composites. *J. Frict. Wear* **2010**, *31*, 281–287. [CrossRef]

18. Savchenko, N.L.; Sevostyanova, I.N.; Utyaganova, V.R.; Gnyusov, S.F. Physicochemical Aspects of Contacting in a WC–(Fe-Mn-C)/Steel Hybrid Sliding Pair. *AIP Conf. Proc.* **2018**, *2053*, 040084. [CrossRef]

19. Gnyusov, S.F.; Fedin, E.A.; Tarasov, S.Y. The effect of counterbody on tribological adaptation of an electron beam deposited HSS M2 steel coating in a range of sliding speeds and normal loads. *Tribol. Int.* **2021**, *161*, 107109. [CrossRef]

20. Sharma, S.K.; Kumar, B.V.M.; Kim, Y.-W. Tribology of WC reinforced SiC ceramics: Influence of counterbody. *Friction* **2019**, *7*, 129–142. [CrossRef]

21. Liu, Y.; Erdemir, A.; Meletis, E.I. A study of the wear mechanism of diamond like carbon films. *Surf. Coat. Technol.* **1996**, *82*, 48–56. [CrossRef]

22. Basu, S.N.; Sarin, V.K. Oxidation behavior of WC-Co. *Mater. Sci. Eng.* **1996**, *A209*, 206–212. [CrossRef]

23. Carlton, H.; Huitink, D.; Hong, L. Tribochemistry as an Alternative Synthesis Pathway. *Lubricants* **2020**, *8*, 87. [CrossRef]

24. Savchenko, N.L.; Kul'kov, S.N. Friction and wear of Y-TZP and Y-TZP-Al_2O_3 ceramics in high-speed sliding on steel. *J. Frict. Wear* **2009**, *30*, 444–448. [CrossRef]

25. Savchenko, N.L.; Sablina, T.Y.; Melnikov, A.G.; Kul'kov, S.N. Behavior of the submicrocrystalline Y-TZP-Al_2O_3 composite in dry friction with steel. *Powder Metall. Met. Ceram.* **2013**, *51*, 577–583. [CrossRef]

26. Cai, L.; Huang, Z.; Hu, W.; Lei, C.; Zhai, H.; Zhou, Y. Dry sliding behaviors and friction surface characterization of $Ti_3Al_{0.8}Si_{0.2}Sn_{0.2}C_2$ solid solution against S45C steel. *Ceram. Int.* **2019**, *45*, 2103–2110. [CrossRef]

27. Wo, S.; Huang, Z.; Cai, L.; Hu, W.; Wang, Y.; Zhou, Y.; Zhai, H. High strengthening effects and excellent wear resistance of $Ti_3Al(Si)C_2$ solid solutions. *Int J. Appl. Ceram. Technol.* **2019**, *16*, 2398–2408. [CrossRef]

28. Huang, Z.; Xu, H.; Zhai, H.; Wang, Y.; Zhou, Y. Strengthening and tribological surface self-adaptability of Ti_3AlC_2 by incorporation of Sn to form $Ti_3Al(Sn)C_2$ solid solutions. *Ceram. Int.* **2015**, *41*, 3701–3709. [CrossRef]

29. Xu, H.; Huang, Z.; Zhai, H.; Li, M.; Liu, X.; Zhou, Y. Fabrication, Mechanical Properties, and Tribological Behaviors of $Ti_3Al_{0.8}Sn_{0.4}C_2$ Solid Solution by Two-time Hot-pressing Method. *Int. J. Appl. Ceram. Technol.* **2014**, *12*, 783–789. [CrossRef]

30. Ravikiran, A. Wear quantification. *J. Tribol.* **2000**, *122*, 650–656. [CrossRef]

31. Pędzich, Z. Tungsten Carbide as an Reinforcement in Structural Oxide-Matrix Composites. In *Tungsten Carbide—Processing and Applications*; IntechOpen: London, UK, 2012. Available online: https://www.intechopen.com/chapters/41528 (accessed on 19 December 2012). [CrossRef]